Signal Detection on Euclidean Groups: Applications to DNA Bends, Robot Localization, and Optical Communication

Kevin C. Wolfe, *Member, IEEE*, and Gregory S. Chirikjian, *Fellow, IEEE*

Abstract—Three problems from disparate application areas are presented and solved here using a unified framework: 1) estimating the bend angle induced in DNA by a bound ligand such as a transcription factor or anti-cancer drug; 2) determining the intent of a mobile robot by observing its trajectories corrupted by environmental noise; 3) estimating the bit-error probability function associated with phase noise in optical communication systems, and the associated problem of filter design. In all three problems, probability densities on the group of proper rigid-body motions of the plane contain a hidden signal that needs to be detected in order to advance the particular application area. Stochastic differential equations and corresponding Fokker-Planck equations describing random processes that evolve on this group (the Euclidean group) are used to model each of these problems, and methods from harmonic analysis and Lie theory are used to write approximate solutions. From these 'forward' models the desired 'signal' (i.e., an element, or a path, in the Euclidean group is extracted) to infer desired physical parameters from data.

Index Terms—Bent DNA, exponential coordinates, group Fourier analysis, phase noise, planar Euclidean group, robot localization.

I. INTRODUCTION

T HREE seemingly unrelated problem areas are addressed in this paper using a common set of mathematical techniques built on classical Lie theory, noncommutative harmonic analysis, and stochastic modeling. Though methods of classical engineering mathematics (matrix algebra, ordinary and partial differential equations, Fourier analysis, etc.) are heavily used in signal processing, methods from differential geometry and abstract algebra such as the representation theory of Lie groups, analysis of stochastic sample paths on group manifolds, and hybrid results that combine information theory and Lie-group theory have been rare in the signal processing literature until recently [1]–[3]. Therefore, in addition to solving the three problems described below, an additional goal of this presentation

is to provide an exposition of methods that may find yet other applications.

The first of the problems addressed here is that of finding the angle induced by a drug or protein that binds to DNA at an a priori known location along the length of a DNA segment of known composition. Our methodology is demonstrated with numerical data generated to model experimental data collection via atomic force microscope, as described in [4]. In this context bent DNA molecules float down to a planar substrate after a ligand binds and induces a bend. When each bent DNA molecule lays flat on the planar substrate, it is modeled as a planar persistent random walk, and our goal is to extract the hidden signal (the relative rigid-body motion describing the angle of the induced bend) from an ensemble of hundreds of such paths. The angle itself can be quite subtle and in general cannot be distinguished by observing a single DNA shape due to stochastic shape fluctuations. Yet such subtle bends are believed to have important biophysical consequences. These sorts of structural changes in DNA can be caused by a number of proteins and compounds. In particular, a number of agents are known to induce bending in DNA [5]–[14] as demonstrated in Fig. 1. These changes can affect critical processes within a cell. For example, many cancer drugs such as cisplatin target DNA and induce bending and other structural changes which can disrupt transcription and replication. If the cell is unable to repair the damaged nucleotides, this bending can lead to apoptosis (cell death) [15].

The second problem addressed here is that of robot localization as described in [16], [17]. Consider a simple mobile robot such as a unicycle or 'kinematic cart' (i.e., a two-wheeled robot like a motorized wheelchair) for which the wheels roll without slipping. We ask the following question: Suppose that the robot and an external observer (such as an overhead camera) have the same dictionary of intended maneuvers of the robot (e.g., go straight for 1 second, follow a clockwise or counterclockwise circular arc of fixed radius for 1 second, etc.), and due to noise in observations, and in the robot's execution of its intended trajectory, can the observer infer the robot's intent and diagnose failure? Developing methodologies to solve these sorts of problems have the potential to endow automated systems with greater error correction capabilities, and represent a merger between the theory of Lie groups in the sense of the methods described in this paper, and information theory (where the robot's intent can be thought of as a message sent to the observer through a noisy channel involving the mechanics of the robot and its interaction with the environment, as well as any interference, limits in resolution, and measurement noise

K. C. Wolfe is with the Research and Exploratory Development Department, Johns Hopkins University Applied Physics Laboratory, Laurel, MD 20723 USA (e-mail: kevin.wolfe@jhuapl.edu).

G. S. Chirikjian is with the Department of Mechanical Engineering, Johns Hopkins University, Baltimore, MD 21218 USA (e-mail: gregc@jhu.edu).
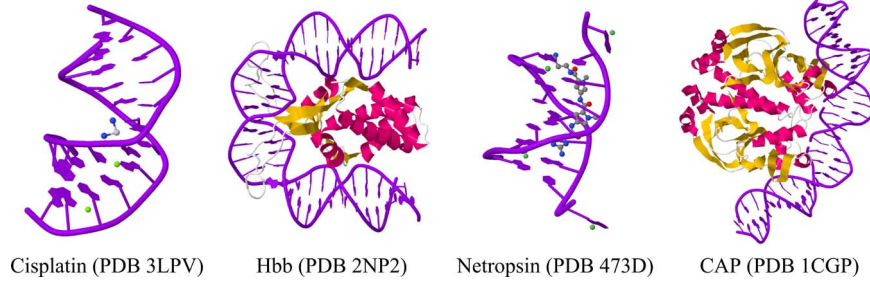
Fig. 1. Four examples of DNA bending. Images generated from PDB data [20] using Jmol [21]. (PDB IDs: 3LPV [15], 2NP2 [22], 473D [23], 1CGP [24]).

on the side of the observer). We show that essentially the same stochastic model that describes the shape of DNA on a planar substrate can be used to describe the stochastic trajectory of the robotic cart, and extracting the intent of the robot is essentially the same problem, subject to the same solution methods, as extracting the bend angle from ensembles of DNA configurations.

The third problem also involves variations on the same mathematical theme in a completely different physical scenario. In optical communication systems, spontaneous emissions of photons in the laser cavity lead to limitations in the amount of information that can be transmitted via fiber-optic cable. This is referred to as the "phase-noise" problem [18], [19]. Associated with phase noise is a stochastic differential equation describing a process that evolves on the Euclidean group of the plane. Solving the corresponding Fokker-Planck equation provides a means for analysis of the bit-error function when a given filter is used. Having efficient methods for solving these equations for a given filter opens the opportunity to investigate the inverse problem of filter design. Here the filter is the analogous quantity to the bend angle or the robot path.

The remainder of this article is organized in the following manner. Section II provides an overview of the planar Euclidean motion group that will be used throughout the paper including the exponential map, Jacobian and adjoint matrices, irreducible unitary representations of the motion group, and the noncommutative Fourier transform. Section III explains how to define left-invariant stochastic differential equations and associated Fokker-Planck equations, and how to solve them. The methods reviewed in these two sections will be used throughout the rest of the paper. Section IV reviews the elastic-filament model and techniques for solving the Fokker-Planck equation associated with it, discusses how the bend is introduced to the elastic model and how the desired probability density functions are obtained, and presents the statistical method for comparing the modeled distributions and sampled data. This section also illustrates the effectiveness of the methods using numerical simulations. Section V discusses two other problems using the same mathematical framework: (1) inferring the intent of a mobile robot with a priori knowledge of its dictionary of maneuvers and physical characteristics; and (2) the phase-noise problem in coherent fiber-optic communication systems. Section VI compares two approaches used to generate distributions that result from the stochastic differential equations. Section VII provides conclusions and directions for future efforts.

II. REVIEW OF SE(2)

The (special) Euclidean group of planar motions, $SE(2)$ is the semidirect product of the plane, $\mathbb{R}^2$, and the special orthogonal group of 2×2 matrices, $SO(2)$. Elements of $SE(2)$ can be represented using 3×3 homogeneous transformation matrices of the form

$$g = \begin{pmatrix} R & \mathbf{t} \\ \mathbf{0}^T & 1 \end{pmatrix} \qquad (1)$$

for

$$R = \begin{pmatrix} \cos(\theta) & -\sin(\theta) \\ \sin(\theta) & \cos(\theta) \end{pmatrix} \in SO(2),$$

$\mathbf{t} = (x, y)^T$, and $\mathbf{0} = (0, 0)^T$. The group operation is then matrix multiplication. The translational portion of g can also be expressed in polar coordinates as $\mathbf{t} = (r \cos(\phi), r \sin(\phi))^T$.

A. Infinitesimal Motion

Associated with the group $SE(2)$ is the Lie algebra $se(2)$ which consists of matrices of the form

$$Z = z_1 E_1 + z_2 E_2 + z_3 E_3 \qquad (2)$$

for

$$E_1 = \begin{pmatrix} 0 & -1 & 0 \\ 1 & 0 & 0 \\ 0 & 0 & 0 \end{pmatrix}, E_2 = \begin{pmatrix} 0 & 0 & 1 \\ 0 & 0 & 0 \\ 0 & 0 & 0 \end{pmatrix},$$

and

$$E_3 = \begin{pmatrix} 0 & 0 & 0 \\ 0 & 0 & 1 \\ 0 & 0 & 0 \end{pmatrix}.$$

A bijective mapping $\vee : se(2) \to \mathbb{R}^3$ and the reverse mapping $\wedge : \mathbb{R}^3 \to se(2)$ are respectively defined by the equations

$$Z^\vee \doteq \begin{pmatrix} z_1 \\ z_2 \\ z_3 \end{pmatrix} = \mathbf{z} \text{ and } \mathbf{z}^\wedge \doteq Z. \qquad (3)$$

Given a rigid-body motion, $g(s)$, parameterized by arc length or time, the "velocity" as experienced in a body-fixed frame can be taken as

$$g^{-1} \frac{dg}{ds} = \begin{pmatrix} R^T \frac{dR}{ds} & R^T \frac{d\mathbf{t}}{ds} \\ \mathbf{0}^T & 0 \end{pmatrix} \in se(2). \qquad (4)$$

These velocities can be separated into a rotational and translational component. If

$$\boldsymbol{\xi} = \begin{pmatrix} \xi_1 \\ \xi_2 \\ \xi_3 \end{pmatrix} = \left(g^{-1} \frac{dg}{ds} \right)^{\vee},$$

then ξ_1 represents the rotational velocity and $(\xi_2, \xi_3)^T$ represents the body-fixed translational velocity.

B. The Exponential Map and Adjoints

Let $\mathbf{z} \in \mathbb{R}^3$ and $Z = \mathbf{z}^{\wedge} \in se(2)$ The matrix exponential, $\exp(\cdot)$, is a map $\exp : se(2) \to SE(3)$ defined by

$$\exp(Z) = \begin{pmatrix} \cos(z_1) & -\sin(z_1) & \frac{[z_2 \sin(z_1) + z_3(-1+\cos(z_1))]}{z_1} \\ \sin(z_1) & \cos(z_1) & \frac{[z_2(1-\cos(z_1)) + z_3 \sin(z_1)]}{z_1} \\ 0 & 0 & 1 \end{pmatrix}.$$
$$(5)$$

We will often denote the 2×2 block at the upper left in $\exp(Z)$ as R, which is a rotation matrix. For $z_1 = 0$ the exponential becomes

$$\exp(Z) = \begin{pmatrix} 1 & 0 & z_2 \\ 0 & 1 & z_3 \\ 0 & 0 & 1 \end{pmatrix}. \tag{6}$$

In a similar fashion the matrix logarithm, $\log(\cdot)$, can be defined to take any element from $SE(2)$ to an element in the subset of $se(2)$ defined by the condition $-\pi < z_1 < \pi$. Restricting the discussion to these subsets of $SE(2)$ and $se(2)$ makes both the exponential and logarithm invertible. And since the set defined by $z_1 = \pi$ in $SE(2)$ constitutes a set of measure zero, the difference is inconsequential when integrating against smooth probability densities.

Adjoint operators are commonly used for both $SE(2)$ and $se(2)$. The adjoint operator for Lie groups can be defined to satisfy

$$\mathrm{Ad}(g) Z^{\vee} = \log^{\vee}(g \circ \exp(Z) \circ g^{-1}) \tag{7}$$

where $\log^{\vee}$ is the composition of $\log$ and $\vee$. For $SE(2)$, this operator is then

$$\mathrm{Ad}(g) = \begin{pmatrix} 1 & \mathbf{0}^T \\ C\mathbf{t} & R \end{pmatrix} \text{ where } C = \begin{pmatrix} 0 & 1 \\ -1 & 0 \end{pmatrix}. \tag{8}$$

C. Jacobian Matrices

Given any parametrization of $SE(2)$ defined by a coordinate vector $\mathbf{q} = (q_1, q_2, q_3)^T$, such as exponential coordinates (z_1, z_2, z_3) or Cartesian coordinates (θ, x, y), the associated left-invariant Jacobian matrix is

$$J(\mathbf{q}) \doteq \left[\left(g^{-1} \frac{\partial g}{\partial q_1} \right)^{\vee}, \ \left(g^{-1} \frac{\partial g}{\partial q_2} \right)^{\vee}, \ \left(g^{-1} \frac{\partial g}{\partial q_3} \right)^{\vee} \right].$$

Explicit expressions for the Jacobians for $SE(2)$ and other Lie groups can be found in [2] and references therein.

To within an arbitrary scaling constant, c, the bi-invariant integration measure can be expressed in coordinates as $dg =$

$c \cdot |\det J(\mathbf{q})| dq_1 dq_2 q_3$. We choose $c = 1/4\pi^2$ so as to make the $SE(2)$-Fourier reconstruction formula and Parseval equality have a simple appearance.

When g is expressed in coordinates as $g(\mathbf{q})$ then the left-invariant "Lie derivatives" of any function $f(g)$, expressed as $\tilde{f}(\mathbf{q}) = f(g(\mathbf{q}))$, are of the form

$$(\tilde{E}_i f)(g) \doteq \left. \frac{d}{dt} f(g \circ \exp(tE_i)) \right|_{t=0} = \mathbf{e}_i^T [J(\mathbf{q})]^{-T} (\nabla_{\mathbf{q}} \tilde{f}) \tag{9}$$

where $\nabla_{\mathbf{q}} \tilde{f} = [\partial \tilde{f}/\partial q_1, \partial \tilde{f}/\partial q_2, \partial \tilde{f}/\partial q_3]^T$.

III. STOCHASTIC DIFFERENTIAL EQUATIONS AND FOKKER-PLANCK EQUATIONS

A. Left-Invariant Stochastic Differential Equations and Fokker-Planck Equations

Throughout this paper, we focus on left-invariant Stratonovich stochastic differential equations on $SE(2)$ of the form

$$\left(g^{-1} dg \right)^{\vee} = \mathbf{a}(t) dt + B(t) d\mathbf{w} \tag{10}$$

where $d\mathbf{w}$ is a vector of uncorrelated unit-strength white noise. The above expression is coordinate free, but it is sometimes useful to introduce coordinates. In this case, (10) can be written as the coordinate-dependent Stratonovich equation

$$J(\mathbf{q}) d\mathbf{q} = \mathbf{a}(t) dt + B(t) d\mathbf{w}$$

or, equivalently,

$$d\mathbf{q} = [J(\mathbf{q})]^{-1} \mathbf{a}(t) dt + [J(\mathbf{q})]^{-1} B(t) d\mathbf{w}. \tag{11}$$

Detailed derivation of the corresponding Fokker-Planck equation can be found in [2], [25], resulting in

$$\frac{\partial f}{\partial t} = -\sum_i a_i \tilde{E}_i f + \frac{1}{2} \sum_{j,k} \left(\sum_l B_{jl} B_{kl} \right) \tilde{E}_j \tilde{E}_k f. \tag{12}$$

This expression, which is independent of coordinates, can be made coordinate dependent by evaluating each $\tilde{E}_i$ using (9) and replacing $f(g;t)$ with $f(g(\mathbf{q});t)$.

In particular, if (θ, x, y) coordinates are used, evaluating (12) with (9) and the parameters

$$\mathbf{a} = [0, 0, h(t)]^T \text{ and } B_{11} = \sqrt{D} \text{ and } B_{jk} = 0 \text{ otherwise}$$

gives

$$\frac{\partial f}{\partial t} = -h(t) \left(-\sin\theta \frac{\partial f}{\partial x} + \cos\theta \frac{\partial f}{\partial y} \right) + \frac{1}{2} D \frac{\partial^2 f}{\partial \theta^2}. \tag{13}$$

The initial conditions are $f(g;0) = \delta(g)$. If the notation $f(g(\theta, x, y); t) = \tilde{f}(\theta, x, y; t)$ is used, then $\tilde{f}(\theta, x, y; 0) = \delta(x)\delta(y)\delta(\theta)$. The term in parenthesis in (13) is $\tilde{E}_3 f$ expressed in coordinates, $\tilde{E}_1 f$ is $\partial \tilde{f}/\partial \theta$, and $\tilde{E}_1^2 f$ is $\partial^2 \tilde{f}/\partial^2 \theta$.

For details regarding derivations of the above equations, and inter-conversion between Stratonovich and Itô forms, see [2] and the associated online addenda. An alternative derivation

of (12) using Gangolli-McKean injection and the Itô SDE formalism is also possible, as described in [26], [27]. Rigorous and thorough treatments of SDEs on manifolds can be found in [28]–[30]. The added structure afforded by the Lie-group nature of $SE(2)$ makes the formulation somewhat easier than in the more general case of manifolds.

One can imagine extensions to (10) in which white noise is replaced by Levy noise. In this case, methods described in [31], [32] would become relevant. However, for this paper we limit the discussion to white noise forcing.

B. Fourier-Based Solution Methods

The group Fourier transform and inversion formula for $G = SE(2)$ can be written as

$$\hat{f}(p) = \int_G f(g)U(g^{-1}, p)dg \tag{14}$$

and

$$f(g) = \int_{\hat{G}} \mathrm{tr}[\hat{f}(p)U(g, p)]d(p) \tag{15}$$

where p is a "frequency" parameter from the unitary dual of G (denoted as $\hat{G}$), $d(p) = p\,dp$ (to within a normalizing constant), and $\{U(g, p)|p \in \hat{G}\}$ is a complete set of irreducible unitary representation matrices [33], [34]. Formulas (14) and (15) generalize to wide classes of unimodular groups including all finite and compact Lie groups (in which case $\hat{G}$ becomes discrete and $d(p)$ becomes a counting measure), $SE(n)$, $SL(n, \mathbb{R})$, $SL(n, \mathbb{C})$, the Poincaré groups, and the Heisenberg groups. However, our concern here is only with $SE(2)$, for which $\hat{G} = \mathbb{R}_{>0}$. In analogy with the classical Fourier transform, the above transform has associated operational properties. For example,

$$(\widehat{\tilde{E}_i f})(p) = W_i(p)\hat{f}(p, s) \tag{16}$$

where

$$\tilde{E}_i f(g) = \left(\frac{d}{dt}f(g \circ \exp(tE_i))\right)\Bigg|_{t=0} \tag{17}$$

is a Lie derivative and can be thought of as a directional derivative in the direction of E_i. Explicitly,

$$W_i(p) = \left(\frac{d}{dt}U(\exp(sE_i), p)\right)\Bigg|_{s=0}.$$

For $SE(2)$, these infinite-dimensional matrices are

$$[W_1]_{mk}(p) = -jk\delta_{m,k} \tag{18}$$

$$[W_2]_{mk}(p) = \frac{jp}{2}[\delta_{k,m+1} + \delta_{n,m-1}] \tag{19}$$

$$[W_3]_{mk}(p) = \frac{p}{2}[\delta_{k,m-1} - \delta_{k,m+1}]. \tag{20}$$

When polar coordinates are used for g, the irreducible representation matrices, $U(g, p)$, for $SE(2)$ are

$$U_{km}(g(\theta, r, \phi), p) = j^{m-k}e^{-j[m\theta + (k-m)\phi]}J_{m-k}(pr). \tag{21}$$

$J_q(\cdot)$ is the qth-order Bessel function, $j = (-1)^{(1/2)}$, and matrices are indexed such that $m, k \in \mathbb{Z}$.

The operational properties in (20) make the group Fourier transform an ideal tool for analyzing diffusions on the group since the diffusion equation is converted to a system of linear ODEs in Fourier space.

C. The Gaussian Solution

1) Moments of Probability Density Functions on Lie Groups: While the definition of a probability density function (pdf) follows directly from pdfs defined over $\mathbb{R}^n$, concepts of mean and covariance on matrix Lie groups are not as straight-forward. However, for pdfs that are relatively concentrated, definitions used for mean and covariance have been extended from those commonly used for pdfs on $\mathbb{R}^n$ [35]–[37]. The mean $\mu \in G$ of a pdf $f(g)$ can be defined such that

$$\int_G \log^\vee(\mu^{-1}g)f(g)dg = \mathbf{0}. \tag{22}$$

This concept of mean, which should not be confused with other concepts such as those presented recently in [3], has some particularly useful properties for our application, as described below.

The covariance matrix Σ for these concentrated pdfs can be defined using

$$\Sigma = \int_G \log^\vee(\mu^{-1}g)\left(\log^\vee(\mu^{-1}g)\right)^T f(g)dg. \tag{23}$$

This too should not be confused with other concepts of covariance that are reviewed in [2], [38], [39].

Along these lines, a pdf for Lie groups has been developed that was inspired by the normal distribution on $\mathbb{R}^n$ [25]. This distribution has been called a Gaussian on exponential coordinates and is given by

$$f(g; \mu, \Sigma) = \frac{1}{c(\Sigma)}\exp\left(-\frac{1}{2}\left[\log^\vee(\mu^{-1}g)\right]^T\Sigma^{-1}\log^\vee(\mu^{-1}g)\right). \tag{24}$$

Here $c(\Sigma)$ is a normalizing factor that ensures that $f(g; \mu, \Sigma)$ is a pdf. When the covariance is small this normalizing factor can be approximated as

$$c(\Sigma) \approx (2\pi)^{n/2}|\det(\Sigma)|^{1/2}$$

where n is the dimension of $\log^\vee(g)$. For $SE(2)$, $n = 3$. In related work, this approach has also been taken for $SE(3)$ in which case $n = 6$ [25].

2) Propagation of Mean and Covariance: As we will demonstrate in subsequent sections, the convolution of pdfs can be used to "piece together" distinct distributions. For example, if two actions are described by their respective pdfs. The convolution of the two pdfs gives the distribution that describes performing the first action followed directly by the second action. The convolution of two functions, $f_1(g)$ and $f_2(g)$, on a Lie group is given by

$$(f_1 * f_2)(g) = \int_G f_1(h)f_2(h^{-1} \circ g)dh. \tag{25}$$

It is often convenient to determine the mean and covariance $(\mu_{1*2}, \Sigma_{1*2})$ of this third distribution given the mean and covariance of the two contributing pdfs (μ_1, Σ_1) and (μ_2, Σ_2). If

$f_1(g)$ and $f_2(g)$ are "concentrated" pdfs centered around μ_1 and μ_2, respectively, then several closed-form approximations have been given for μ_{1*2} and Σ_{1*2}. The details of these derivations are given in [40] and [41] for Euclidean motion groups, such as $SE(2)$ and $SE(3)$. If $\|\Sigma_i\| \ll 1$ and $\|\log(\mu_i)\| = O(1)$, then a "first-order"[1] approximation can be used reliably. This first-order propagation gives the following approximations for mean and covariance:

$$\mu_{1*2} = \mu_1 \circ \mu_2 \tag{26}$$

and

$$\Sigma_{1*2} = Ad(\mu_2^{-1})\Sigma_1 Ad^T(\mu_2^{-1}) + \Sigma_2. \tag{27}$$

Second-order closed-form approximations are also available in [40] and [41] for situations when the underlying distributions are more diffuse; however, these approximations will not be explored here.

In the small-time limit, and starting with the initial conditions $\Sigma(0) = \mathbb{O}$ and $\mu(0)$ equal to the group identity element, repeated application of the propagation formulas for the mean and covariance can be iterated to give integrals for these quantities:

$$\mu(t) = \exp\left(\int_0^t \mathbf{a}^\wedge d\tau\right) \tag{28}$$

and

$$\Sigma_{1*2}(t) = \int_0^t Ad(\mu^{-1}(\tau))BB^T Ad^T(\mu^{-1}(\tau))d\tau. \tag{29}$$

When $\Sigma(t)$ is small enough, the resulting Gaussian distribution solves the diffusion equation because if $f_t(g) = f(g;t)$, then $f_{t_1+t_2}(g) = (f_{t_1} * f_{t_2})(g)$.

In many numerical applications, the Gaussian solution outlined here may be advantageous to use over the Fourier method described earlier (and which will be demonstrated in the next section). In particular when $\Sigma(t)$ is small enough to justify the use of the Gaussian solution, the distribution being described is very concentrated. Such a compact distribution requires that a larger number of frequencies be used to numerically integrate the Fourier inversion formula. The increased number of frequencies means that larger truncations are required to adequately represent the infinite dimensional Fourier matrices. Both of these require significantly higher computational time when compared with evaluating the closed-form Gaussian solution. However, as the distribution becomes more dispersed, smaller truncation sizes and few frequencies can be used to faithfully represent the distribution using the Fourier approach. In addition, more dispersion leads to violations of the assumptions that underlie (26) and (27). The difference of these two methods is described further in Section VI.

IV. INEXTENSIBLE ELASTIC-ROD MODEL OF DNA

DNA is a relatively stiff molecule and is often modeled as a homogeneous elastic rod. For fairly long DNA fragments (longer than about 100 nm), this worm-like chain model provides a description that correlates well with experiments such as force

---

[1] First-order here refers to the number of terms kept in the Baker-Campbell-Hausdorff expansion of $\exp(X)\exp(Z)$ where X and Z are elements of the associated Lie algebra. Additional details of the precise definition can be found in [40] and [41].
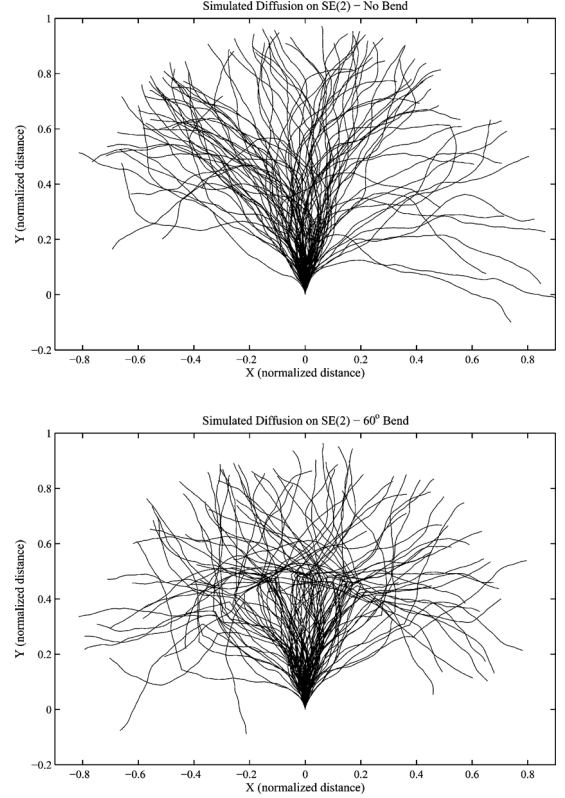

Fig. 2. Simulated ensembles of stochastic trajectories for (30) with $\eta = 0.7$: (top) Without a bend; (bottom) With a $60°$ bend. Bends are assumed to occur with equal frequency in the positive and negative direction.

spectroscopy [42]–[44]. While this model can be expressed in a general fashion to include axial elasticity along the length of the molecule, it is often simplified and assumed to be inextensible because of the stiff nature of DNA. This assumption results in a model with Brownian forcing on the orientation only. For DNA constrained to planar surfaces, this model can be written as a stochastic differential equation (SDE) of the form

$$\boldsymbol{\xi}ds = \begin{pmatrix} 0 \\ 0 \\ 1 \end{pmatrix} ds + \begin{pmatrix} \sqrt{2\eta} \\ 0 \\ 0 \end{pmatrix} dw. \tag{30}$$

This model has a straight backbone such that the unperturbed path has a constant drift or "velocity" in the y direction. Here s represents the arc length of the molecule and η corresponds with the flexibility of the DNA. The top plot in Fig. 2 shows a set of paths generated using this model for $\eta = 0.7$.

The Fokker-Planck equation associated with this model is

$$\frac{\partial f}{\partial s} = \left(\eta\left(\tilde{E}_1\right)^2 + \tilde{E}_3\right)f. \tag{31}$$

The Fokker-Planck equation represents the probability density function describing the elastic filament model for a fixed value of s. If we let L represent the full length of the DNA filament, $f(g;s)$ will represent the pdf of g for $s \in [0, L]$. Assuming Dirac delta initial conditions, $f(g;0) = \delta(g)$, the solution to (31) provides the distribution of relative positions and orientations with respect to the proximal end. It should be noted that the formulation given in (30) and (31) does not account for excluded-volume effects. However, in the unconstrained plane,

these models are generally assumed to be valid for a few persistence lengths.

There are several methods that can be used to solve the Fokker-Planck equation given in (31). However, for relatively long filaments, the group Fourier transform has a number of properties that make it useful for obtaining the corresponding pdf.

For a homogeneous filament model such as (30), the operation properties allow us to use the matrix exponential to solve the differential equation that results from applying the Fourier transform to (31).

In particular, we can use (14), (15), and (16), to write

$$\frac{d\hat{f}}{ds} = \left(\eta \left(W_1(p) \right)^2 + W_3(p) \right) \hat{f} \qquad (32)$$

where $W_i(p)$'s are determined using (20).

Using the matrix exponential to solve this differential equation in Fourier space then yields [45]

$$\hat{f}(p; s) = \exp \left(s \left(\eta \left(W_1(p) \right)^2 + W_3(p) \right) \right). \qquad (33)$$

The probability distribution function can then be recovered using the inverse Fourier transform defined in (15). This can also be written as a double summation,

$$f(g; s) = \sum_{m,k \in \mathbb{Z}} \int_0^\infty \hat{f}_{mk}(p; s) U_{km}(g, p) p \, dp. \qquad (34)$$

A. Adding a Static Bend

In order to compare the statistics of experimentally sampled bent DNA data with those of the elastic model, we must add a bend to the middle of the elastic model. This is done using convolution which allows us to take the distributions for two lengths fixed lengths and obtain the overall distribution that would results from serially connecting the two fragments. For two fragments with lengths L_1 and L_2 this convolution is defined to be

$$f(g; L_1, L_2) = (f_{L_1} * f_{L_2})(g)$$
$$= \int_G f(h; L_1) f(h^{-1} \circ g; L_2) dh. \qquad (35)$$

The use of the Fourier transform as defined in (14) to solve the Fokker-Planck equation in (31) is particularly convenient when the distribution of interest results from the convolution of functions. This is because the Fourier transform of the convolution of two functions can be written

$$\widehat{(f_1 * f_2)} = \hat{f}_2 \hat{f}_1. \qquad (36)$$

Using convolution, we can write the overall distribution for a strand of DNA with a bend in the middle as

$$f(g; L_1) * b(g) * f(g; L_2)$$

where b(g) describes the bend or twist that is induced. A number of forms for $b(g)$ were given by Zhou and Chirikjian in [46]. For the purposes of this work we will use a bend distribution of the form

$$b(g; \theta_0) = \frac{\delta(r)}{r} \delta(\theta - \theta_0) \qquad (37)$$

where $\delta(\cdot)$ is the Dirac delta and θ_0 is the bend angle. More information on the form of this bend function in $SE(2)$ can be found in E.1.3 of [34]. The Fourier transform of this static bend can be expressed as

$$\hat{b}(p; \theta_0) = \int_G \frac{\delta(r)}{r} \delta(\theta - \theta_0) U(g^{-1}, p) d(g)$$
$$= \int_{\phi=0}^{2\pi} \int_{\theta=0}^{2\pi} \int_{r=0}^\infty \frac{\delta(r)}{r} \delta(\theta - \theta_0)$$
$$\times U^*(g, p) r \, dr \, d\phi \, d\theta \qquad (38)$$

where * denotes the Hermitian conjugate. The elements of $\hat{b}(p; \theta_0)$ can then be written as

$$\hat{b}_{mk}(p; \theta_0) = \int_{\phi=0}^{2\pi} \int_{\theta=0}^{2\pi} \int_{r=0}^\infty \delta(r) \delta(\theta - \theta_0) \overline{j^{m-k}}$$
$$\cdot e^{j[m\theta + (k-m)\phi]} J_{m-k}(pr) dr \, d\phi \, d\theta. \qquad (39)$$

Using the fact that

$$J_{m-k}(0) = \begin{cases} 1 & \text{if } m = k \\ 0 & \text{otherwise} \end{cases}. \qquad (40)$$

Equation (39) can be simplified to

$$\hat{b}_{mk}(p; \theta_0) = \int_{\phi=0}^{2\pi} \int_{\theta=0}^{2\pi} \delta(\theta - \theta_0) e^{jm\theta} \delta_{m,n} d\phi \, d\theta$$
$$= 2\pi \int_{\theta=0}^{2\pi} \delta(\theta - \theta_0) e^{jm\theta} \delta_{m,n} d\theta$$
$$= e^{jm\theta_0} \delta_{m,k}. \qquad (41)$$

In summary, if we want to determine the distribution of the inextensible elastic model with total length $L_1 + L_2$ and a θ_0 bend at $s = L_1$ we can substitute

$$\hat{f}_{L_1 * \theta_0 * L_2}(p) = \exp \left(L_2 \left(\eta \left(W_1(p) \right)^2 + W_3(p) \right) \right) \hat{b}(p; \theta_0)$$
$$\cdot \exp \left(L_1 \left(\eta \left(W_1(p) \right)^2 + W_3(p) \right) \right) \qquad (42)$$

into the inverse Fourier transform given by (15) (or (34)). Then since this distribution provides a full description of the relative end-to-end motion of the model, a number of quantities of interest can be computed, including end-to-end distance and end-to-end orientation distributions. Next we will compute some of the marginals of this distribution and demonstrate how they may be used to determine model parameters of interest.

B. Marginal Distributions and Statistical Inference of Parameters

1) Marginalization Over θ and ϕ: While the full distribution of the model is available with respect to all of the coordinates of g as described above, accurate measurements of things such as orientation or position may be more difficult to obtain experimentally. For example, when measurements are taken using the AFM techniques described in [45] and [4] the relative orientation between ends is not easily measured. Therefore, marginalization can be used to obtain distributions that are only functions of the coordinates of interest. Because the orientation, θ, is not as easily measured experimentally, we can marginalize over it to obtain a distribution that is only a function of position. This can be done by looking at the inverse Fourier transform from
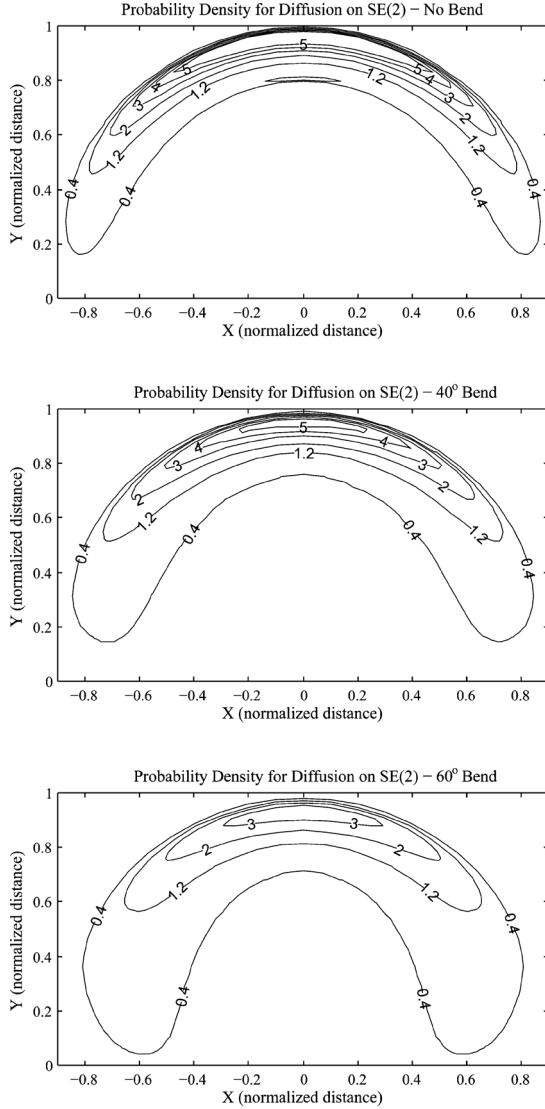
Fig. 3. Distribution of the distal end position of the model relative to the proximal end for $\eta = 0.7$: (top) Without a bend; (middle) With a 40° bend; (bottom) With a 60° bend. These plots have been marginalized over orientation, θ. Also, bends are assumed to occur with equal frequency in the positive and negative directions.

(34) marginalized over θ which can be obtained by looking at the integral

$$\int_0^{2\pi} f(g(\theta, r, \phi); s)d\theta$$

$$= \sum_{m,k \in \mathbb{Z}} \int_{p=0}^{\infty} \hat{f}_{mk}(p; s) \left(\int_{\theta=0}^{2\pi} U_{km}(g, p)d\theta \right) pdp. \quad (43)$$

Here the inner integral on the right-hand side can be expressed as

$$\int_0^{2\pi} U_{km}(g, p)d\theta = \int_0^{2\pi} j^{m-k} e^{-j[m\theta + (k-m)\phi]} J_{m-k}(pr)d\theta$$

$$= 2\pi j^{-k} e^{-jk\phi} J_{-k}(pr)\delta_{0,m}. \quad (44)$$

This comes about as $\int_0^{2\pi} e^{-jm\theta}d\theta = 0$ for $m \neq 0$. Substituting (44) into (43) yields

$$\int_0^{2\pi} f(g; s)d\theta = 2\pi \sum_{n \in \mathbb{Z}} \int_0^{\infty} \hat{f}_{0k}(p; s) j^{-k} e^{-jk\phi} J_{-k}(pr) p \, dp. \quad (45)$$

Distributions resulting from marginalization over θ are given in Fig. 3 for three different bend angles: 0°, 40°, and 60°. For

these contour plots $L_1 = L_2 = 0.5$ and $\eta = 0.7$. This flexibility value was chosen as it closely resembles what was seen in the AFM images given in [45] when the length of the imaged DNA fragments was normalized. Also, because of the random overall orientation of DNA samples during experimental imaging, these distributions assume that both positive and negative values of θ_0 occur with equal frequency.

It should further be noted that because the Fourier-space operator matrices in (18)–(20) are infinite dimensional, they need to be truncated before they can be exponentiated. For these plots (and the remaining analysis) the W_i's were truncated to 101×101 before exponentiation. The resulting matrices were further reduced to 51×51 before the inverse Fourier transform was applied. It is clear from these distributions that increasing the bend angle, θ_0, results in distributions that are more spread out. As one would expect, a similar spreading effect can be seen for increases in the flexibility parameter, η.

Marginalization allows us to reduce the measurement uncertainty by relying on quantities in which we are most confident. In [45], covariances in three dimensions were explored for both the simulated and experimental ensembles; however, the sample covariances for the experimental data have additional uncertainty associated with them because of manipulation that needs to be performed to obtain the proximal and distal orientations. On the other hand, end-to-end distances, which contain less information, can be more accurately determined. The use of polar coordinates helps to facilitate obtaining a pdf of end-to-end distance values as this can be obtained by marginalizing over both θ and ϕ. Integrating (45) over ϕ yields a distribution in just r. This is shown to be equal to

$$\int_{\phi=0}^{2\pi} \int_{\theta=0}^{2\pi} f(g; s)d\theta d\phi =$$

$$= \int_{\phi=0}^{2\pi} 2\pi \sum_{k \in \mathbb{Z}} \int_{p=0}^{\infty} \hat{f}_{0k}(p; s) j^{-k} e^{-jk\phi}$$

$$\times J_{-k}(pr)pdpd\phi$$

$$= 2\pi \sum_{k \in \mathbb{Z}} \int_{p=0}^{\infty} \hat{f}_{0k}(p; s) j^{-k} \left(\int_{\phi=0}^{2\pi} e^{-jk\phi}d\phi \right)$$

$$\times J_{-k}(pr)pdp. \quad (46)$$

The inner integral on the right-hand side is computed as

$$\int_{\phi=0}^{2\pi} e^{-jk\phi}d\phi = 2\pi \delta_{0,k}. \quad (47)$$

Substituting this into (46) gives

$$\int_{\phi=0}^{2\pi} \int_{\theta=0}^{2\pi} f(g; s)d\theta d\phi = 4\pi^2 \int_{p=0}^{\infty} \hat{f}_{00}(p; s) J_0(pr)pdp. \quad (48)$$

Finally, we can substitute the center entry in (42) into this equation and use the Fourier inversion formula (41) to obtain the end-to-end distance distribution.

2) Statistical Inference of Parameters: In the model defined by (30) with fixed length and a bend at the midpoint, the two parameters of interest are the flexibility, η, and the angle of the central bend, θ_0. We can now look at how the end-to-end distribution in (48) may be used to obtain values for these two parameters given two sets of sampled or experimental data. Let us assume that we are given two sets of normalized end-to-end

distances for DNA constrained to the plane: one for unperturbed DNA and one for DNA with an induced bend in the middle. We will assume that (1) the DNA fragments are well modeled using (30) (or equivalently (31)) and (2) the bend only causes a local structural change. Then, we can use the sampled data for unperturbed DNA to determine the value of the flexibility parameter η. This value can be coupled with the second data set to infer the bend angle θ_0.

Let $f(r; \eta, \theta_0)$ be the distribution obtained using (48) and (42) for $L_1 = L_2 = 0.5$ and fixed values of η and θ_0. Also, let D^{Unbent} and D^{Bent} be the sets of normalized end-to-end distance values for the naked/unperturbed DNA and bent DNA data, respectively. We can then use the sum of log-likelihoods to obtain η^*, the value of η that best describes D^{Unbent}. This value is taken as

$$\eta^* = \arg \max_{\eta} \mathcal{L}(\eta, 0, D^{Unbent}) \tag{49}$$

where

$$\mathcal{L}(\eta, \theta_0, D) = \sum_{r_i \in D} \log \left(f(r_i; \eta, \theta_0) \right). \tag{50}$$

Using this value for the flexibility parameter allows us to determine θ_0^* in a similar manner. Specifically, we can take θ_0^* to be

$$\theta_0^* = \arg \max_{\theta_0 \in [0, \pi]} \mathcal{L}(\eta^*, \theta_0, D^{Bent}). \tag{51}$$

The search space for θ_0^* is limited to $[0, \pi]$, because $f(r; \eta, \theta_0) = f(r; \eta, -\theta_0)$. Moreover, it is assumed that if the bend angle in the model is taken to be θ_0, then approximately half of the fragments will exhibit a bend of θ_0 and the other half $-\theta_0$.

To demonstrate the effectiveness of these methods two series of numerical experiments were conducted. For all of the data sets, 1,000 sample trajectories were numerically generated using (30). All trajectories had unit total length $(L_1 + L_2 = 1)$ and all bends occurred at $L_1 = 0.5$. Fig. 2 demonstrates several smaller ensembles of simulated trajectories for different values of θ_0.

For the first set of simulations, unbent DNA was simulated using $\theta_0 = 0$, the flexibility of each data set was varied, and the resulting best fit as given by (49) was determined. The values of η used to generate the simulated DNA fragments varied from 0.5 to 0.95. The resulting values of η^* correlated very well as shown in Fig. 4. Fig. 5 demonstrates how $\mathcal{L}(\eta, 0, D^{Unbent})$ varies with η for three of these trials. It is clear that $\mathcal{L}(\eta, 0, D^{Unbent})$ is a smooth function with respect to η and has a single maximum (η^*) very close to the value of η used to generate the sample set.

The second set of simulations used a constant flexibility of $\eta = 0.7$ and varied θ_0 for each data set. Using the method described above, θ_0^* was determined using (51) and the flexibility, $\eta^* = 0.693$, that was determined for the unbent data set that had been generated using $\eta = 0.7$. Bend values were varied from $10°$ to $80°$. Fig. 6 shows the bend value used and the resulting θ_0^*. Again, the values that maximize (50) are very close to those used to generate the simulated ensembles. As was shown for η, Fig. 7 demonstrates how $\mathcal{L}(0.693, \theta_0, D^{Bent})$ varies with θ_0 for three data sets with different degrees of bending.

Determining structural characteristics of DNA is important, particularly when developing drugs and processes that rely on locally changing these characteristics. One example of such local changes are bends that are induced by agents such as
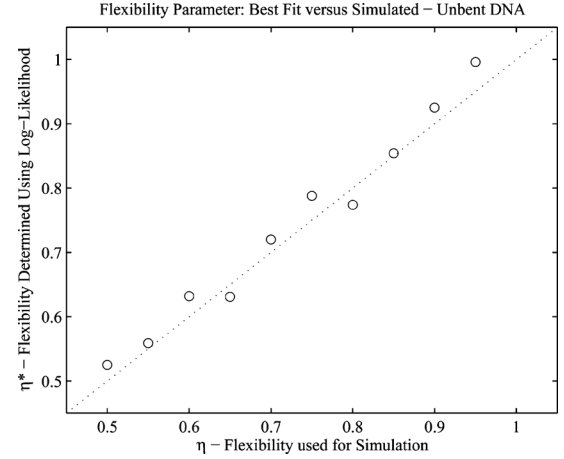

Fig. 4. Best fit flexibility parameter (η^*) for several data sets generated with different values of η.
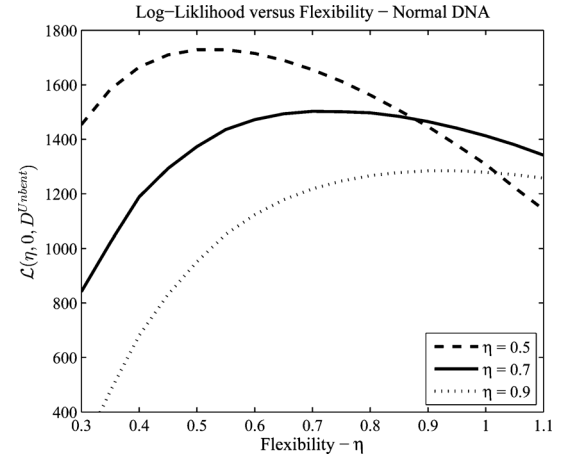

Fig. 5. The log-likelihood function is plotted with respect to flexibility for the unbent DNA model for three values of η. The three plots peak near the flexibility value used in each of the simulated data sets.
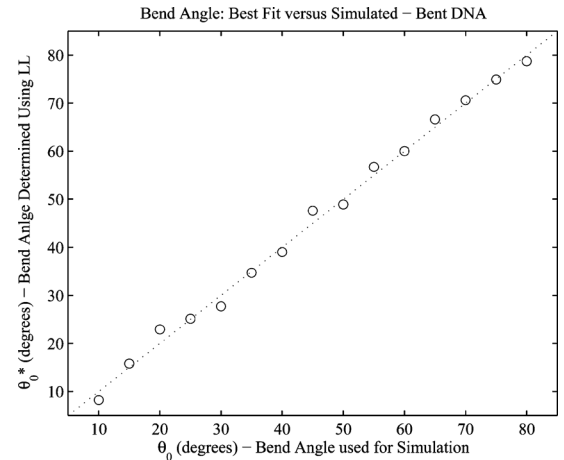

Fig. 6. Best fit bend angle (θ_0^*) for several data sets generated with different values of θ_0 and a fixed value of $\eta = 0.7$. These bend angles were determined using $\eta^* = 0.693$, the value inferred from an unbent data set with $\eta = 0.7$.

drugs and proteins. Characterizing these bends and measuring the angle of the bend induced have proven to be difficult given the currently available sensing modalities. In this work we presented a classic elastic model for DNA diffusing on the plane and developed a method for determining the bend angle by comparing the distributions of the model with experimental
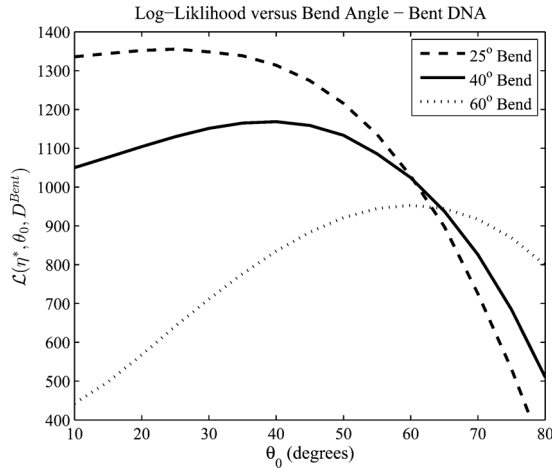
Fig. 7. The log-likelihood function is plotted with respect to bend angle for the DNA model with an induced bend in the middle for three bend angles. The plots peak near the bend value used in the corresponding simulated data set.

or sampled data. This method is intended to be used with experimental measurements of end-to-end distances of DNA constrained to a planar substrate. The ability to collect such data has been previously established.

The model presented assumes a fixed value for the angle of the bend. Future efforts may focus on modifying the model to account for variability in this angle. We may also investigate modifying the model to account for sequence dependent flexibility.

V. APPLICATIONS IN ROBOTICS AND OPTICAL COMMUNICATION SYSTEMS

A. Inferring Intent From Observations of Mobile Robots

It has been shown that a good model for a unicycle-like mobile robot subjected to noise can be given by the same SDE that describes DNA [16]. Indeed, many nonholonomic mobile robots including the unicycle, the kinematic cart, and the Dubins kinematic car model all have similarities. The stochastic forcing here can enter due to roughness of the terrain and other effects. Therefore, a robot that executes an open loop trajectory will never exactly follow the intended path. Such paths could be constructed from segments of motion primitives such as straight line segments and circular arcs that are stitched together to form a continuous trajectory. Each primitive can be viewed as a letter in an alphabet, and a whole trajectory can be viewed as a word. Suppose that an overhead camera records images of the robot, and this camera is connected to a computer equipped with a priori knowledge of the motion primitives. That is, the robot and computer share the same dictionary. If the computer's job is to diagnose the health of the robot through its performance, it can ask the robot to perform a task, observe the performance, and compare that performance to normal behavior. The range of normal behaviors can be modeled via SDEs with a noise level that is determined a priori from physical experiments, and the ensemble can be characterized by the solutions of the Fokker-Planck equation. Then, if the robot is performing within normal limits, the intended motion (or 'signal') can be detected and recovered from the camera/computer system using inference methods. In particular, if the robot is asked to move

forward with a speed $h(t)$, then the Fokker-Planck equation describing the probability density of its evolution will be exactly the same as in the Phase-Noise problem described below, and when $h(t) = 1$, it will be exactly the same as in the DNA problem. If it is asked to move in a more complicated pattern in the plane, this will change the drift equation, but the same methods will apply. That is, drift terms corresponding to motion in a straight line or circular arc have constant coefficients, and the overall Fourier matrix for a whole 'word' can be written as a product of matrix exponentials, one for each 'letter.' These ideas are explained in more detail in [1], [2], [17] which draw a number of connections between signals on Lie groups, the communication of noise-corrupted versions of those signals, and the extension of information-theoretic inequalities to the Lie-group setting.

B. Phase Noise and Filter Design in Coherent Optical Communications

The two major types of optical communication systems are "direct" detection systems and "coherent" detection systems. Here we discuss how a Fokker-Planck equation on the Euclidean group arises in the context of coherent detection systems, and the corresponding signal detection problems.

Coherent systems have some theoretical advantages over direct detection systems, but this comes at the cost of increased complexity, and a problem called *laser phase noise*. In a coherent detection system, light is added to the incoming modulated signal as part of the detection process via a local oscillator, even if subsequent processing and demodulation ignore the phase and frequency, as is the case of envelope detectors [47]. Adding the input from the local oscillator to weak conventional intensity modulation increases sensitivity of the system, resulting in what is called a "weakly coherent system."

In contrast to direct detection systems, coherent detection systems have the potential to detect the phase, frequency, amplitude, and polarization of the incident light signal. Therefore, in principle, information can be transmitted via phase, frequency, amplitude, or polarization modulation. Of all the obstacles preventing coherent techniques from being used widely in practice, laser phase noise is one of the largest. The phase of the light emitted from a semiconductor laser exhibits random fluctuations due to spontaneous emissions in the laser cavity [48]. This phenomenon is commonly referred to as phase noise. Because there are only about 10^4 photons in the active region of a semiconductor laser, the phase of the light is significantly perturbed by just one spontaneous photon. If there were no spontaneous emission, the output light spectrum would consist of delta functions (each delta function $\delta(\omega - \omega_i)$ corresponding to one longitudinal mode at frequency ω_i). As a result of random spontaneous emissions, the spectrum is no longer a sum of delta functions, but instead the spectrum is broadened and has a finite nonzero linewidth around each ω_i. The amount of phase noise is directly related to its so-called linewidth, the 3 dB linewidth of its power spectrum density. The spectral width of a modern microwave oscillator is less than 1 Hz, that of a DFB laser is 1 MHz. As of a few years ago, the best GaAsInp DFB lasers had a linewidth less than 1 KHz [49], [50].

Phase noise has two important adverse effects on the performance of coherent optical communications. One effect is the broadening of the linewidth of a light source output mentioned
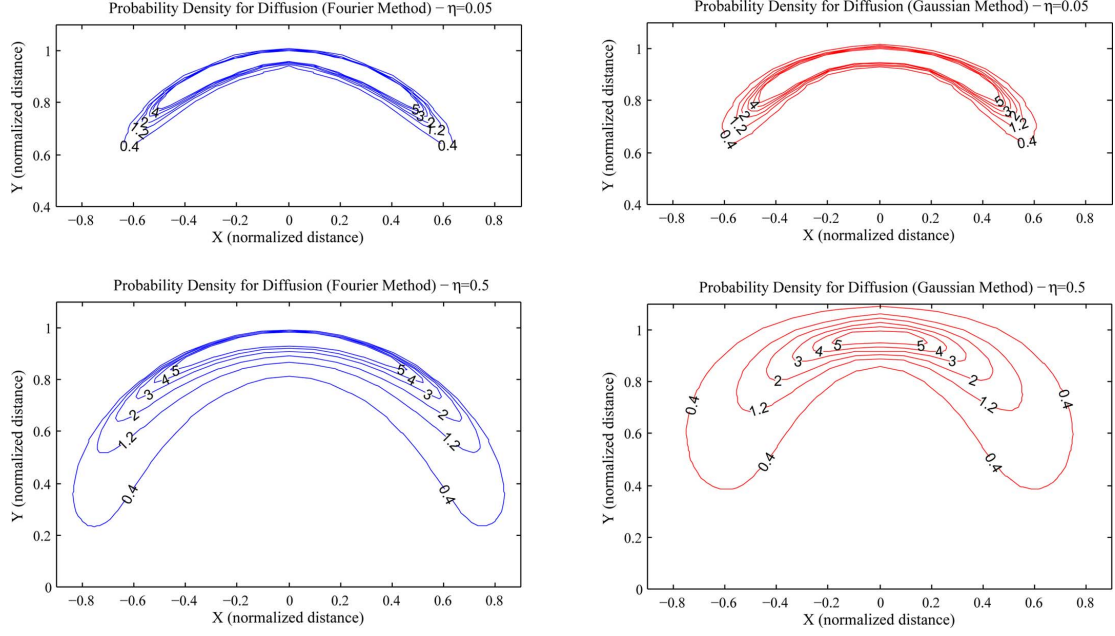
Fig. 8. A comparison of the two approaches for obtaining distributions for the diffusion model with a 30° bend in the middle. Two values of η are provided to represent concentrated (top) and dispersed (bottom) distributions.

above. This results in inefficient use of the available bandwidth and causes interchannel interference and thus necessitates wider channel spacing. The second effect is that phase noise directly corrupts the phase or frequency of a modulated carrier. It makes the correct retrieval of the transmitted data bits (i.e., "signal detection") more difficult for the receiver. The system sensitivity is degraded, as measured by the BER (bit error rate) [51]. For a BER, this necessitates an increase in received signal power compared to the ideal situation (power penalty). In some cases the presence of phase noise creates a lower limit on the probability of a bit error (BER floor) below which the system cannot operate.

Some methods to alleviate the influence of phase noise have been proposed by [18], [52]. They involve receiver structures and signaling mechanisms that are relatively insensitive to phase uncertainty. As was pointed out in detail by [53] and [54], to evaluate the phase noise effects on coherent optical systems, the main issue is to find the statistical characterization of the output of the IF filter. Analytical models that describe the relationship between phase noise and the filtered signal are found in [19], [53]–[55]. In particular, the Fokker-Planck approach represents the most rigorous description of phase noise effects [54], [56], [57]. To better apply this approach to system design and optimization, an efficient and powerful computational tool is necessary. The solution of the Fokker-Planck equation has been described as a difficult problem, and herein lies the connection with our paper.

Ultimately, in coherent optical communication systems, the limitation on the amount of information that can be transmitted due to laser phase noise is described using (13) as described in [19], [53]–[55], [58]. This is the same equation as the DNA equation, where now instead of $h(t)$ being constant, it now describes the IF filter that can be chosen (i.e., "designed"). In this context, x and y are the real and imaginary parts of the noisy part of any signal being sent by the laser over an optical fiber, and θ is the phase variable. D is the magnitude of phase

noise in the coherent optical system used to send the signal $z(t) = x(t) + iy(t)$. Therefore, studying the relationship between this design choice and the resulting pdf is a sort of signal detection problem. The methods presented in this paper for computing $f(g; t)$ may therefore serve as a design tool wherein candidates for $h(t)$ are evaluated so as to shape, to the extent possible, the resulting pdf $\tilde{f}(x, y, \theta)$ and the associated marginal densities of interest in coherent optical communication systems.

VI. COMPARISON OF THE FOURIER AND GAUSSIAN APPROACHES

As discussed previously, the Fourier-based and Gaussian on exponential coordinate solutions each have different strengths and limitations. The Gaussian approach is much less computationally intensive, but limited to concentrated distributions. The Fourier-based approach is more general, but is very computationally intensive for these same concentrated distributions. The approach taken in Section IV relied primarily on the Fourier-based approach because of the disperse nature of the underlying phenomenon. However, if the diffusion coefficient were smaller, as would be expected in the case of mobile robots, the Gaussian method would also be applicable.

We will briefly demonstrate these differences using the bent DNA model, but the results are equally applicable to the mobile robot and phase noise problems discussed. If we consider (30) along with the integral forms of $\mu(s)$ and $\Sigma(s)$ given in (28) and (29), the mean and covariance for $s = L$ are found to be

$$\mu(L) = \begin{pmatrix} 1 & 0 & 0 \\ 0 & 1 & L \\ 0 & 0 & 1 \end{pmatrix} \qquad (52)$$

and

$$\Sigma(L) = \begin{pmatrix} 2\eta L & -\eta L^2 & 0 \\ -\eta L^2 & \frac{2}{3}\eta L^3 & 0 \\ 0 & 0 & 0 \end{pmatrix}. \qquad (53)$$
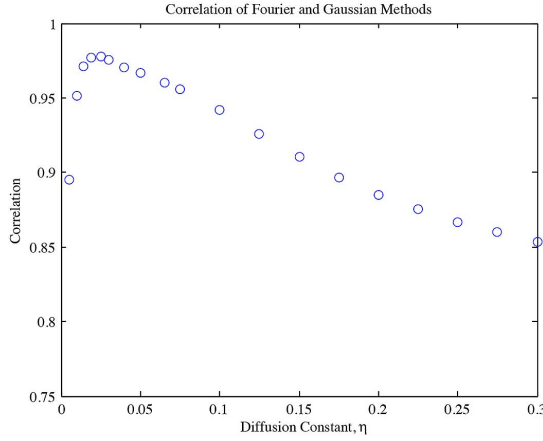
Fig. 9. Correlation between distributions resulting from the Fourier and Gaussian approaches. These distributions were marginalized over orientation before the difference was determined.

We can then use (26) and (27) with a mean and covariance representing a discrete bend to find $\mu_{L1*b*L2}$ and $\Sigma_{L1*b*L2}$. The moments representing this bend are $\Sigma_b = \mathbb{O}$ and

$$\mu_b(\theta_0) = \begin{pmatrix} \cos(\theta_0) & -\sin(\theta_0) & 0 \\ \sin(\theta_0) & \cos(\theta_0) & 0 \\ 0 & 0 & 1 \end{pmatrix}.$$

This propagated mean and covariance were used with (24) to generate the plots given in Fig. 8 which all contain a bend of $30°$. As before, $L_1 = L_2 = 0.5$. These plots qualitatively demonstrate that the two methods provide similar distributions for small values of diffusion, but the pdfs diverge as η grows.

We can also demonstrate this by looking at the correlation of the resulting pdfs. Fig. 9 shows the correlation of the two pdfs that have been marginalized over orientation with respect to the diffusion coefficient η. This plot also shows that over a range of values of the diffusion parameter the distributions are very similar, but if the diffusion constant becomes too small, then the Fourier method breaks down, and if the diffusion constant becomes too large the Gaussian approximation degrades.

VII. Conclusion

In this work, we presented methods for extracting signals from probability density functions associated with degenerate diffusions on Euclidean groups. Such problems arise in three very different scenarios: 1) finding the induced bend angle in an inextensible elastic filament model of DNA that is confined to a planar substrate, but exhibits planar diffusion; 2) inferring intent of a kinematic cart with a known dictionary of maneuvers; 3) characterizing the bit-error function in the laser phase noise problem and providing a methodology for testing the effects of different filters. These methods relied on several useful properties of the group Fourier transform, and the Gaussian distribution in exponential coordinates.

In some of these scenarios the full distributions are used, whereas in others marginal densities are required. For example, in the bent DNA problem, densities were marginalized to obtain distributions over end-to-end distance as this quantity is more easily measured than the full relative pose of the proximal and distal ends of DNA. Given these parameterized distributions and end-to-end distance data sets for bent and unbent DNA, we

demonstrated how log-likelihood methods can be utilized to determine the angle of the bend present in the bent DNA. The wide variety of values of flexibility, η, and bend angle, θ_0, used in the numerical experiments highlight how effective these methods may be for experimental data collected from samples with very different structural properties. However, because the shape of the functions in Figs. 5 and 7 are more concave downward for lower values of η and θ_0, we can assume that these methods are more sensitive to changes in these regions. As such, we believe that these methods are best suited for stiffer molecules with larger bend angles.

Finally, we explored the differences and similarities between the Fourier-based and Gaussian of exponential coordinates approaches. Further exploration of which applications lend themselves to either approach should be performed. In particular, determining methods for transitioning from one method to the other as distributions spread out are of interest.

References

[1] G. S. Chirikjian, "Information-theoretic inequalities on unimodular Lie groups," *J. Geometric Mech.*, vol. 2, no. 2, pp. 119–158, 2010.

[2] G. S. Chirikjian, *Stochastic Models, Information Theory, and Lie Groups*. Boston, MA, USA: Birkhäuser, 2012, vol. 2.

[3] S. Said and J. H. Manton, "Extrinsic mean of Brownian distributions on compact Lie groups," *IEEE Trans. Inf. Theory*, vol. 58, no. 6, pp. 3521–3535, Jun. 2012.

[4] C. Rivetti, M. Guthold, and C. Bustamante, "Scanning force microscopy of DNA deposited onto mica: Equilibration versus kinetic trapping studied by statistical polymer chain analysis," *J. Molec. Biol.*, vol. 264, no. 5, pp. 919–932, 1996.

[5] D. Crothers, M. Gartenberg, and T. Shrader, "DNA bending in protein-DNA complexes," *Meth. Enzymol.*, vol. 208, pp. 118–146, 1991.

[6] J. Griffith, A. Makhov, L. Zawel, and D. Reinberg, "Visualization of tbp oligomers binding and bending the hiv-1 and adeno promoters," *J. Molec. Biol.*, vol. 246, no. 5, pp. 576–584, 1995.

[7] J. Pérez-Martin and M. Espinosa, "Protein-induced bending as a transcriptional switch," *Science*, vol. 260, pp. 805–807, 1993.

[8] W. Rees, R. Keller, J. Vesenka, G. Yang, and C. Bustamante, "Evidence of DNA bending in transcription complexes imaged by scanning force microscopy," *Science*, vol. 260, no. 5114, pp. 1646–1649, 1993.

[9] D. Allen, A. Makhov, M. Grilley, J. Taylor, R. Thresher, P. Modrich, and J. Griffith, "Muts mediates heteroduplex loop formation by a translocation mechanism," *EMBO J.*, vol. 16, no. 14, pp. 4467–4476, 1997.

[10] R. Lobell and R. Schleif, "DNA looping and unlooping by AraC protein," *Science*, vol. 250, no. 4980, pp. 528–533, 1990.

[11] O. Wong, M. Guthold, D. Erie, and J. Gelles, "Interconvertible lac repressor-DNA loops revealed by single-molecule experiments," *PLoS Biol.*, vol. 6, no. 9, pp. 2028–2042, 2008.

[12] S. L. Adhya and S. Garges, *RNA polymerases and associated factors*. New York, NY, USA: Academic, 2003, vol. 370.

[13] C. Rivetti, M. Guthold, and C. Bustamante, "Wrapping of DNA around the e. coli RNA polymerase open promoter complex," *EMBO J.*, vol. 18, no. 16, pp. 4464–4475, 1999.

[14] K. Rippe, P. von Hippel, and J. Langowski, "Action at a distance: DNA-looping and initiation of transcription," *Trends in Biochem. Sci.*, vol. 20, no. 12, pp. 500–506, 1995.

[15] R. C. Todd and S. J. Lippard, "Structure of duplex DNA containing the cisplatin 1, 2-{pt $(NH_3)_2$}$^{2+}$-d (gpg) cross-link at 1.77 a resolution," *J. Inorgan. Biochem.*, vol. 104, no. 9, pp. 902–908, 2010.

[16] Y. Zhou and G. Chirikjian, "Probabilistic models of dead-reckoning error in nonholonomic mobile robots," in *Proc. IEEE Int. Conf. Robot. Autom.*, 2003, pp. 1594–1599.

[17] G. S. Chirikjian, "Information theory on Lie groups and mobile robotics applications," in *Proc. IEEE Int. Conf. Robot. Autom.*, 2010, pp. 2751–2757.

[18] G. Foschini, L. Greenstein, and G. Vannucci, "Noncoherent detection of coherent lightwave signals corrupted by phase noise," *IEEE Trans. Commun.*, vol. 36, no. 3, pp. 306–314, Mar. 1988.

[19] D. Bond, "The statistical properties of phase noise," *British Telecom. Technol. J.*, vol. 7, no. 4, pp. 12–17, 1989.

[20] H. M. Berman, J. Westbrook, Z. Feng, G. Gilliland, T. N. Bhat, H. Weissig, I. N. Shindyalov, and P. E. Bourne, "The protein data bank," *Nucleic Acids Research*, vol. 28, no. 1, pp. 235–242, 2000.

[21] "Jmol: An open-source Java viewer for chemical structures in 3D," [Online]. Available: http://www.jmol.org

[22] K. Mouw and P. Rice, "Shaping the Borrelia burgdorferi genome: Crystal structure and binding properties of the DNA-bending protein Hbb," *Molec. Microbiol.*, vol. 63, no. 5, pp. 1319–1330, 2007.

[23] N. Abrescia, L. Malinina, and J. Subirana, "Stacking interaction of guanine with netropsin in the minor groove of d (CGTATATACG) 21," *J. Molec. Biol.*, vol. 294, no. 3, pp. 657–666, 1999.

[24] S. Schultz, G. Shields, and T. Steitz, "Crystal structure of a CAP-DNA complex: The DNA is bent by 90 degrees," *Science*, vol. 253, no. 5023, pp. 1001–1007, 1991.

[25] W. Park, Y. Wang, and G. Chirikjian, "The path-of-probability algorithm for steering and feedback control of flexible needles," *Int. J. Robot. Res.*, vol. 29, no. 7, pp. 813–830, 2010.

[26] R. Gangolli, "On the construction of certain diffusions on a differentiable manifold," *Z. Wahrscheinlichkeitstheorie und verw. Geb.*, vol. 2, pp. 406–419, 1964.

[27] H. McKean, *Stochastic Integrals*. New York, NY, USA: Academic, 1969.

[28] K. D. Elworthy, *Stochastic Differential Equations on Manifolds*. Cambridge, U.K.: Cambridge Univ. Press, 1982.

[29] M. Emery, *Stochastic Calculus in Manifolds*. New York, NY, USA: Springer-Verlag, 1989.

[30] N. Ikeda and S. Watanabe, *Stochastic Differential Equations and Diffusion Processes*, 2nd ed. Amsterdam, The Netherlands: North-Holland, 1989.

[31] D. Applebaum and H. Kunita, "Lévy flows on manifolds and Lévy processes on Lie groups," *J. Math. Kyoto. Univ.*, vol. 33, pp. 1103–1123, 1993.

[32] M. Liao, *Lévy Processes in Lie Groups*. Cambridge, U.K.: Cambridge Univ. Press, 2004.

[33] G. S. Chirikjian and A. B. Kyatkin, "An operational calculus for the Euclidean motion group with applications in robotics and polymer science," *J. Fourier Anal. Applicat.*, vol. 6, no. 6, pp. 583–606, 2000.

[34] G. S. Chirikjian and A. B. Kyatkin, *Engineering Applications of Noncommutative Harmonic Analysis*. Boca Raton, FL, USA: CRC, 2000.

[35] A. W. Long, K. C. Wolfe, M. Mashner, and G. S. Chirikjian, "The banana distribution is Gaussian: A localization study with exponential coordinates," in *Proc. Robot.: Sci. Syst.*, 2012.

[36] W. Park, Y. Liu, Y. Zhou, M. Moses, and G. Chirikjian, "Kinematic state estimation and motion planning for stochastic nonholonomic systems using the exponential map," *Robotica*, vol. 26, no. 4, pp. 419–434, 2008.

[37] Y. Wang and G. S. Chirikjian, "Error propagation on the Euclidean group with applications to manipulator kinematics," *IEEE Trans. Robot.*, vol. 22, no. 4, pp. 591–602, Aug. 2006.

[38] U. Grenander, *Probabilities on Algebraic Structures*. New York, NY, USA: Dover, 2008.

[39] H. Heyer, *Probability Measures on Locally Compact Groups*. New York, NY, USA: Springer-Verlag, 1977.

[40] A. W. Long, K. C. Wolfe, and G. S. Chirikjian, "Planar uncertainty propagation and a probabilistic algorithm for interception," in *Proc. Workshop Algorith. Foundat. Robot.*, 2012.

[41] Y. Wang and G. S. Chirikjian, "Nonparametric second-order theory of error propagation on the Euclidean group," *Int. J. Robot. Res.*, vol. 27, no. 11–12, pp. 1258–1273, 2008.

[42] C. Bustamante, J. F. Marko, E. D. Siggia, and S. Smith, "Entropic elasticity of lambda-phage DNA," *Science*, vol. 265, no. 5178, pp. 1599–1600, 1994.

[43] C. Bustamante, S. B. Smith, J. Liphardt, and D. Smith, "Single-molecule studies of DNA mechanics," *Current Opinion Struct. Biol.*, vol. 10, no. 3, pp. 279–285, 2000.

[44] P. Nelson, *Biological Physics: Energy, Information, Life*. New York, NY, USA: W. H. Freeman, 2004.

[45] K. C. Wolfe, W. Hastings, S. Dutta, A. W. Long, B. A. Shapiro, T. Woolf, M. Guthold, and G. S. Chirikjian, "Multiscale modeling of double-helical DNA and RNA: A unification through lie groups," *J. Phys. Chem., B*, vol. 116, no. 29, pp. 8556–8572, 2012.

[46] Y. Zhou and G. Chirikjian, "Conformational statistics of bent semiflexible polymers," *J. Chem. Phys.*, vol. 119, no. 9, pp. 4962–4970, Sep. 2003.

[47] L. Kazovsky, S. Benedetto, and A. Willner, *Optical Fiber Communication Systems*. Norwood, MA: Artech House, 1996.

[48] C. Henry, "Theory of linewidth of semiconductor lasers," *IEEE J. Quantum Electron*, vol. 18, pp. 259–264, 1982.

[49] F. Topsoe, "Some inequalities for information divergence and related measures of discrimination," *IEEE Trans. Inf. Theory*, vol. 46, no. 4, pp. 1602–1609, Jul. 2002.

[50] W. Zhang, Y. C. Lai, J. A. R. Williams, C. Lu, L. Zhang, and I. Bennion, "A fibre grating DFB laser for generation of optical microwave signal," *Opt. Laser Technol.*, vol. 32, no. 5, pp. 369–371, 2000.

[51] J. Barry and E. Lee, "Performance of coherent optical receivers," *Proc. IEEE*, vol. 78, no. 8, 1990.

[52] M. Azizoglu and P. Humblet, "Envelope detection of orthogonal signals with phase noise," *J. Lightw. Technol.*, vol. 9, no. 10, pp. 1398–1410, Oct. 1991.

[53] G. Foschini and G. Vannucci, "Characterizing filtered light waves corrupted by phase noise," *IEEE Trans. Inf. Theory*, vol. 34, no. 6, pp. 1437–1448, Nov. 1988.

[54] I. Garrett, D. Bond, J. Waite, D. Lettis, and G. Jacobsen, "Impact of phase noise in weakly coherent systems: A new and accurate approach," *J. Lightw. Technol.*, vol. 8, no. 3, pp. 329–337, Mar. 1990.

[55] G. Foschini, G. Vannucci, and L. Greenstein, "Envelope statistics for filtered optical signals corrupted by phase noise," *IEEE Trans. Commun.*, vol. 37, no. 12, pp. 1293–1302, Dec. 1989.

[56] I. Garrett and G. Jacobsen, "Phase noise in weakly coherent systems," *IEE Proc. J. Optoelectron.*, vol. 136, no. 3, pp. 159–165, Jun. 1989.

[57] X. Zhang, "Analytically solving the Fokker-Planck equation for the statistical characterization of the phase noise in envelope detection," *J. Lightw. Technol.*, vol. 13, no. 8, pp. 1787–1794, Aug. 1995.

[58] Y. Wang, Y. Zhou, D. Maslen, and G. Chirikjian, "Solving the phase-noise Fokker-Planck equation using the motion-group Fourier transform," *IEEE Trans. Commun.*, vol. 54, no. 5, pp. 868–877, May 2006.

Kevin Wolfe (S'10–M'12) received the B.S.M.E. degree in mechanical engineering from The College of New Jersey, Ewing, NJ, USA, in 2007 and the M.S.E. and the Ph.D. degrees in mechanical engineering from Johns Hopkins University, Baltimore, MD, in 2009 and 2012, respectively. He is currently a post doctoral fellow at the Johns Hopkins University Applied Physics Laboratory.

Gregory Chirikjian received the B.A. and B.S. degree in mathematics and engineering mechanics, respectively, from Johns Hopkins University in 1988, the M.S.E. degree in mechanical engineering from Johns Hopkins University in 1988, and the Ph.D. degree in applied mechanics from the California Institute of Technology, Pasadena, CA, in 1992. He is currently a professor of Mechanical Engineering at Johns Hopkins University.